Optical Materials 157 (2024) 116300

Contents lists available at ScienceDirect

Optical Materials

journal homepage: www.elsevier.com/locate/optmat

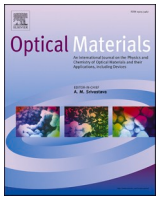

Research Article

Optical properties of CVD-grown multilayer graphene on nickel using spectroscopic ellipsometry

Hervin Maulina [a,b], Eri Widianto [c], Emmistasega Subama [b], Muhammad Riswan [a], Cipto Driyo [a], Dwi Nugraheni Rositawati [d], Fahrudin Nugroho [a], Moh Edi Wibowo [e], Iman Santoso [a,*]

[a] Department of Physics, Faculty of Mathematics and Natural Sciences, Universitas Gadjah Mada, Sekip Utara PO Box BLS 21, Yogyakarta, 55281, Indonesia
[b] Department of Physics Education, Faculty of Teacher Training and Education, Universitas Lampung, Lampung, 35145, Indonesia
[c] Department of Physics, Faculty of Engineering, Universitas Singaperbangsa Karawang, Telukjambe Timur, Karawang, 41361, Indonesia
[d] Department of Physics Education, Faculty of Teacher Training and Education, Sanata Dharma University, Jl. Affandi Mrican Tromol Pos 29, Yogyakarta, 55002, Indonesia
[e] Department of Computer Science, Faculty of Mathematics and Natural Sciences, Universitas Gadjah Mada, Sekip Utara PO Box BLS 21, Yogyakarta, 55281, Indonesia

ARTICLE INFO

Keywords:
Optical properties
Multilayer graphene
Nickel
Spectroscopic ellipsometry

ABSTRACT

Incorporating graphene into relevant technologies requires its integration with commercially suitable substrates. Understanding the interactions between graphene and these substrates is crucial, as graphene serves as an ideal model system for investigating electronic phenomena. In this work, we report the optical properties of multilayer graphene on nickel substrates using spectroscopic ellipsometry. We provide information on the spectral dependence of optical properties of multilayer graphene, such as the complex dielectric constant, refractive index, and optical conductivity in the energy range of 1.6–5.0 eV. The optical conductivity profile obtained from SE analysis showed a symmetrical peak at 4.38 eV, suggesting an interband transition from the π to π^* orbital at the *M* point. The graphene/Ni interaction generated changes in the number of available states below the Fermi level, leading to significant changes in electron density. Our result provides the information essential for understanding relevant research and developing graphene-based optoelectronic applications.

1. Introduction

Graphene, which consists of six carbon atoms in a single-layer hexagonal lattice, has attracted significant interest in materials science following its 2004 discovery because of its outstanding mechanical, electronic, and optical properties [1,2]. At the *K* point of the Brillouin zone, where electrons and holes are present, graphene exhibits a distinctive linear dispersion band structure, as described by the 2D Dirac equation [1–4]. The size, speed, and bandwidth limitations in the semiconductor and optoelectronic industries open up opportunities for graphene to be a promising candidate for developing next-generation devices. Among its outstanding features are the extreme electron mobility that exceeds 10000 $cm^2\ V^{-1}\ s^{-1}$ [5,6], the ability to adjust carrier density through an external electric field [7], and the cooling and heating of carriers on pico- and femtosecond timescales [8]. Graphene is used as a transparent conducting electrode (TCE), increasing the efficiency of photovoltaics [9–11] and TCE for future flexible devices [12–14]. Exploring the potential of graphene as a protective coating, it has an sp^2 carbon allotrope surface that forms an inherent diffusion and a physical barrier between the reactive component and the protected metal [15].

Graphene displays outstanding chemical and thermal stability, remaining steady at exceedingly high temperatures surpassing 1500 °C in an inert environment [16,17]. Additionally, it offers many advantages, including a high optical transparency (approximately 2.3 % absorption) in the visible spectrum, as well as enhanced electrical and thermal conductivity [18–20]. However, experimental samples typically involve doped graphene due to impurities, defects, substrates, and similar factors, deviating from the ideal intrinsic graphene structure [21,22]. Incorporating graphene into relevant technologies requires its integration onto commercially suitable substrates. Understanding the interactions between graphene and substrates is crucial, as graphene serves as a model system ideal for investigating electronic phenomena, including the electron-electron (e-e) and electron-hole (e-h) interaction [23,24].

Several theoretical and experimental studies have been conducted to

* Corresponding author.
E-mail address: iman.santoso@ugm.ac.id (I. Santoso).

https://doi.org/10.1016/j.optmat.2024.116300
Received 9 July 2024; Received in revised form 9 October 2024; Accepted 18 October 2024
Available online 19 October 2024

investigate the attractive properties of graphene on various substrates. For instance, density functional theory calculations have explored graphene adsorption on nickel (Ni) surfaces [25], the modified electronic band structure of monolayer graphite/Ni [26], magnetic and electronic properties of quasi-freestanding graphene on Ni [27], and investigating alterations in the electronic structure of a graphene/Ni [28]. Sutter et al. outlined the electronic structure of few-layer epitaxial graphene on Ru [29], whereas Moritz et al. identified the matching phase structure of graphene on Ru [30]. Wintterlin and Bocquet showcased the electronic structure of metal-graphene systems, where the π band experiences a notable energy downshift compared to free-standing graphene [31]. Pletikosić et al. provided an extensive description of the electronic band structures of graphene on Ir(111) [32]. Walter et al. reported on the electronic band structure of graphene on Cu single-crystal [33]. Consequently, investigating the effects of specific substrates on the superimposed graphene is essential.

The variations in the interfaces between graphene and various metals principally arise from differences in lattice alignment and the interaction between graphene and metal. Regarding lattice alignment, the Ni (111) surface exhibits a high level of similarity with graphene when compared to other transition metals. The similar lattice matching between graphene and Ni allows the formation of a 1 × 1 graphene structure on Ni upon growth at room temperature and standard vacuum conditions. The π bands of graphene exhibit strong hybridization with Ni (111) surface [28]. At the same time, the negligible bonding distance of the initial graphene layer and the lack of distinctive vibrational and electronic signatures of graphene suggest a similar behavior on Ru (0001) [29,30]. In metals demonstrating a relatively robust interaction, the low-index orientations of graphene are often aligned with that of the metal substrate, as shown in chemical vapor deposition (CVD) growth [34,35]. The CVD is the current deposition technique capable of producing graphene in large areas and very high quality. Its compatibility with chip fabrication is crucial for practically implementing graphene-based devices.

Numerous investigations have delved into graphene coated with Ni, examining the evolution of carbon structure and growth kinetics on the Ni(111) surface at various temperatures [36]. Comparative studies have explored direct CVD graphene growth on Ni(111) and polycrystalline Ni films [37]. In addition, a low-temperature CVD was used to create single-layer graphene on Ni(111) with epitaxial growth, all done under ultra-high vacuum conditions [38]. The CVD process has successfully enabled the production of single-layer graphene on nickel droplets [39]. However, it is essential to note that all these studies primarily optimize graphene-coated Ni. Understanding the optical characteristics of graphene on a Ni substrate is crucial for fully harnessing its potential across diverse applications, from optoelectronics to photonics. The interaction between graphene and Ni is crucial in shaping the optical properties of the graphene layer. As researchers continue to unveil the intricate dynamics between graphene and Ni at the optical level, the insights gleaned from this exploration offer substantial potential for advancing the creation of novel devices and technologies. Whether employed in transparent conductive films, sensors, or energy-efficient optoelectronic devices, an enhanced understanding of the optical properties of graphene on Ni presents fresh opportunities for innovation and progress in materials science and engineering.

An in-depth understanding of the optical properties of graphene is essential, especially in designing graphene-based optoelectronic devices and improving their performance. Meanwhile, transmittance and reflectance measurements have determined absorbance and optical conductivity [40,41]. Essential parameters like the dielectric function or optical constants are being extracted from these spectra, which present significant challenges. Several spectroscopic ellipsometry (SE) studies have dedicated considerable efforts to determining the optical properties of graphene [42–49]. SE is one of the most well-established, non-destructive, highly sensitive, and accurate methods of characterizing the optical properties of materials [50,51]. It measures the change in polarization when light is reflected or transmitted through a material. The shift in polarization is represented as the ratio of amplitude (ψ) and phase difference (Δ). In addition, these values can precisely derive essential optical parameters such as complex refractive index ($N \equiv n - ik$), complex dielectric constant ($\varepsilon = \varepsilon_1 - i\varepsilon_2$), optical absorption ($\alpha$), and optical conductivity (σ). Previous optical evaluations often involved monolayer graphene, which are generally small in size and requires intricate experimental procedures [42–49].

Theoretical investigations into the optical properties of graphene using the GW + Bethe Salpeter Equation (BSE) approach have observed resonant excitonic phenomena in graphene [52,53]. Experimentally, resonant excitons have been observed at 4.6 eV and ascribed to electron-hole interactions inside the optical transition from π to π^* orbits at *M*-points [41–43,45–47,54–58]. The optical properties of graphene on standard substrates, such as Si/SiO_2 and quartz, were extensively investigated by SE [42–49,59–62]. Notably, no reports detail the optical properties of CVD graphene grown on Ni substrates. In this work, we present an SE analysis of the optical properties of multilayer CVD graphene on Ni within the energy range of 1.6–5.0 eV. Furthermore, we provide a method for in-depth analysis of the spectroscopic ellipsometry parameters and optical behavior of graphene. This method has the potential to be readily applied to other two-dimensional materials. Our findings reveal the emergence of anomalous optical properties observed in multilayer graphene positioned above a thick Ni substrate.

2. Material and methods

Multilayer CVD graphene on a 10 mm × 10 mm Ni substrate was acquired from Graphene Laboratories Inc, Graphene Supermarket, US (https://www.graphene-supermarket.com/products). They typically consisted of 1–7 layers, with an average thickness of approximately four monolayers. Graphene on Ni was utilized for the study. Raman spectra of the multilayer CVD graphene were captured using a 532 nm laser excitation wavelength, employing a Homemade Raman Spectrometer equipped with a QE Pro High-Performance Spectrometer from Ocean Insight and a Raman probe from Thunder Optics. Morphological and chemical composition analyses, including quantitative analysis of constituent elements, were conducted utilizing a scanning electron microscope with energy-dispersive X-ray spectroscopy (SEM-EDX) on a JEOL JSM-6510LA instrument. The measurements were conducted in the range of 0–20 keV with a voltage of 15 kV and a pixel resolution of 1024 × 768. The probe current emitted electrons and determined secondary or backscattered electrons with an emission of 1 nA.

A rotating-analyzer ellipsometer (RAE) with a spectrometer using a Red Tide USB-650-UV from Ocean Optics was used to investigate optical properties. The measurements were carried out at incident angles of 70° and 75°, respectively, at room temperature, spanning the energy range from 1.6 to 5 eV. The experimental setup for spectroscopic ellipsometry (SE) is schematically depicted in Fig. 1(a), as described in detail in our earlier research [63–66]. SE allows for the accurate determination of ψ and Δ parameters, which are defined by the equation: $\tan(\psi)\exp(i\Delta) = r_p/r_s$, where r_p and r_s denote the complex reflection amplitudes corresponding to *p*- and *s*-polarized light [50]. In this context, ψ represents the amplitude ratio and Δ indicates the phase difference between *p*- and *s*-polarized reflected light.

The optical constants are obtained by modeling the system using Fresnel coefficients specifically designed for multi-layered systems, as depicted in Fig. 1(b). The model includes a Ni bulk layer (layer 4), multilayer CVD graphene (layer 2), and air (layer 0). Given that the multilayer graphene exhibits the step morphology of Ni, we propose the incorporation of extra layers (layer 1 and layer 3) to effectively accommodate the surface roughness of the graphene layer and the interface between the graphene and Ni. The Fresnel equation for reflected light (*p*- and *s*-polarization) at an interface between two layers may be expressed as follows [50,51]:

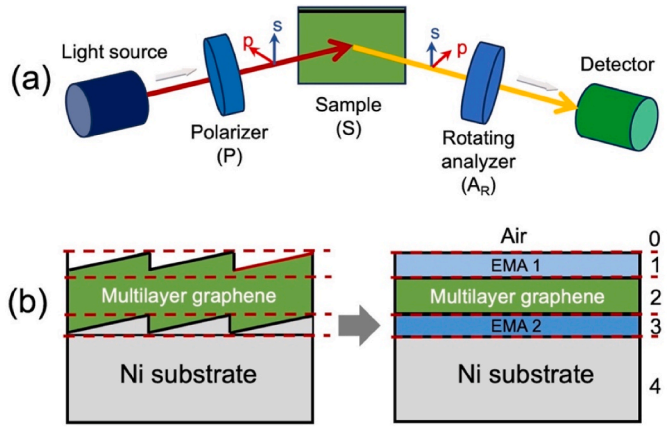

Fig. 1. (a) Schematic illustration of a spectroscopic ellipsometry (SE) setup and (b) Optical model of multilayer CVD graphene on Ni.

$$r_{01,p} = \frac{\sqrt{\varepsilon_1}\cos\theta_0 - \sqrt{\varepsilon_0}\cos\theta_1}{\sqrt{\varepsilon_1}\cos\theta_0 + \sqrt{\varepsilon_0}\cos\theta_1} \tag{1.a}$$

$$r_{01,s} = \frac{\sqrt{\varepsilon_0}\cos\theta_0 - \sqrt{\varepsilon_1}\cos\theta_1}{\sqrt{\varepsilon_0}\cos\theta_0 + \sqrt{\varepsilon_1}\cos\theta_1} \tag{1.b}$$

To calculate the optical constant of the multilayer CVD graphene, the software program IGOR Pro 7 was used to construct a proper isotropic model to fit the ellipsometry data (ψ and Δ). It is generally well known that an ideal thin film with a homogeneous and perfectly flat surface is rare. Thus, many studies mainly involve non-ideal thin films with surface roughness at the top, thickness variations, and optical constants that varied from top to bottom [51,67]. The thickness of Ni substrate is 1 mm, and the optical constants for Ni were obtained from the database: https://refractiveindex.info/. The graphene coverage of this product is about 95 %, with 1–7 layers with an average of 4 monolayer thickness. The thickness of graphene was difficult to see because it was very thin and transparent. We utilized a self-consistent iteration analysis to extract the complex dielectric function and the thickness of films, as in the previous report [65,68]. As long as the iteration is convergent, the initial assumption of these parameters should have little effect on the final acquired values.

First, the dielectric function of multilayer CVD graphene (ε_{MLG}) was fitted into the experimental ψ and Δ data was measured at $\theta = 70^{\circ}$, where the initial value for thickness (d_1) was estimated and set at 2.5 nm. In the next step, the resulting ε_{MLG} was applied to fit the analysis at $\theta = 75^{\circ}$. The ε_{MLG} was fixed and (d_1) was subsequently adjusted into the experimental ψ and Δ data measured at $\theta = 75^{\circ}$. The above procedure was repeated by returning to the data measured at $\theta = 70^{\circ}$ and repeating through the incidence angles, adjusting just one variable at a time while holding the other constant [69]. From the analysis, it is found that the thickness of the multilayer graphene is 2.6 nm, close to the sample specification (average 4 monolayer thickness). If we perform ellipsometry analysis using a data set obtained from different incidence angles or thin film thicknesses, more reliable ellipsometry results can be obtained [50]. To account for the surface (EMA 1) and interface (EMA 2) roughnesses, a Bruggeman effective medium approximation is used, in which the medium is composed of 50 %: 50 %, which is given by

$$f_a\frac{\varepsilon_a - \varepsilon}{\varepsilon_a + \varepsilon} + (1 - f_a)\frac{\varepsilon_b - \varepsilon}{\varepsilon_b + \varepsilon} = 0, \tag{2}$$

where f_a, f_b, ε_a and ε_b are the fraction of air, the fraction of thin film, the complex dielectric constant of air and the complex dielectric constant of the thin film, respectively. From the fitting procedure, the roughness of our multilayer graphene sample is 0.01 nm. To obtain these dielectric constants, we utilize oscillators characterized by the Drude-Lorentz model [50,51]:

$$\varepsilon(\omega) = \varepsilon_\infty + \sum\nolimits_k \frac{\omega_{p,k}^2}{\omega_{0,k}^2 - \omega^2 - i\gamma k\omega} \tag{3}$$

The symbol ε_∞ refers to the dielectric function at high energy, encompassing the contribution from all oscillators at significantly higher energies than those within the observed energy ranges. The parameters $\omega_{0,k}, \omega_{p,k}$ and γ_k represent the eigen (transverse) energy, plasma energy, and line-width associated with the k-th Lorentz oscillator, respectively. The correlation between the optical conductivity $\sigma_1(\omega)$ and the absorption or imaginary part of the dielectric constant, $\varepsilon_2(\omega)$ may be expressed by the following equation:

$$\sigma_1(\omega) = \frac{\omega\varepsilon_2(\omega)}{4\pi} \tag{4}$$

By measuring ψ and Δ, the optical constants of the samples can be calculated. However, this is not a simplistic procedure since the sample must be modelled, and the data produced by the model should be compared to the experimental result while adjusting the parameters, such as optical constants and film thickness. The value that closely matches the experimental data is determined during this iteration procedure by reducing the mean square error (χ^2) [50]:

$$\chi^2 = \chi_{psi}^2 + \chi_{del}^2 \tag{5.a}$$

$$\chi^2 = \frac{1}{\sqrt{M-P-1}}\left\{\sum_{j=1}^{M}\left(\left[\frac{\psi_{exp}(\omega_j) - \psi_{cal}(\omega_j)}{\delta\psi(\omega_j)}\right]^2 + \left[\frac{\Delta_{exp}(\omega_j) - \Delta_{cal}(\omega_j)}{\delta\Delta(\omega_j)}\right]^2\right)\right\} \tag{5.b}$$

where M and P are the number of data and parameters, respectively; ψ_{exp} and ψ_{cal} are the ψ from the experiment and calculation, respectively; Δ_{exp} and Δ_{cal} are the Δ from the experiment and calculation at a specific frequency ω_j, respectively; and ($\delta\psi$, $\delta\Delta$) denotes measurement errors in (ψ, Δ). The mean squared error (MSE or χ^2) of the fit at incident angles of 70° and 75°, the MSE values are 0.075 and 0.039, respectively, which is less than 1, indicating a good fitting result.

3. Results and discussion

We evaluated the structural characteristics of multilayer CVD graphene samples on Ni substrates to verify their quality before optical measurements. Multilayer graphene on Ni has a Raman spectrum with distinctive G and 2D peaks at 1575 cm^{-1} and 2693 cm^{-1}, respectively, and a weak peak at 1345 cm^{-1} linked to defects (D band). The Raman spectrum indicates a multilayer structure with a G to 2D peak intensity ratio greater than two [70,71], as depicted in Fig. 2(a). Our samples' surface morphology and elemental composition results are presented in Fig. 2(b) using SEM-EDX. In Fig. 2(b), a SEM image of the multilayer CVD graphene surface is shown at a magnification of 5000 ×. The image reveals a consistently uniform surface, indicating the high quality of the multilayer CVD graphene, with minimal residue and enhanced brightness observed in regions with wrinkles. The carbon atom concentration is approximately 29.66 %, while nickel constitutes 70.34 %, distributed uniformly across the sample area.

We performed SE measurements at various angles of incidence to examine the dielectric function of multilayer graphene on Ni. Since SE measurements give the real and imaginary components of the dielectric function directly, they are usually favoured. On the other hand, other methods, such as direct reflectivity, need a Kramers-Kronig transformation. Fig. 3(a) and (b) display the experimental data for ψ and Δ corresponding to graphene on Ni, obtained from SE measurements at incident angles of 70° and 75°. Initially, we analyzed these ψ and Δ data by fitting the experimental data to the dielectric model. The black dashed lines represent the best-fit model results, closely matching the experimental data. The optical constants of an optical multilayer system are employed by using the Fresnel coefficients, as shown in Fig. 1(b)

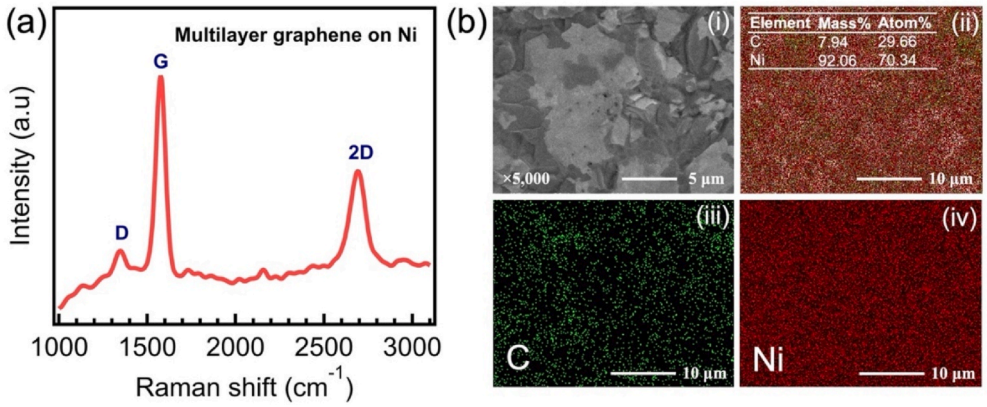

Fig. 2. (a) Raman shift and (b) SEM-EDX elemental mapping image of multilayer CVD graphene on Ni: (i) morphology, (ii) total (insert table for the atomic and mass percentage of various elements), (iii) C, and (iv) Ni.

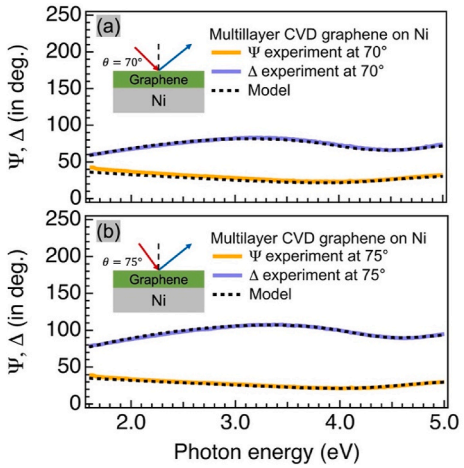

Fig. 3. The SE measurement data (ψ and Δ) of multilayer CVD graphene on Ni at the angle of incident:(a) 70° and (b) 75°.

Fig. 4 illustrates the spectral variation of the optical characteristics of multilayer graphene on Ni. In Fig. 4(a), both the real part (ε_1) and the imaginary part (ε_2) of multilayer graphene on Ni are depicted. The dispersion response of ε_1 showed a positive trend, extending up to 4.2 eV, followed by a transition of a negative trend around 4.5 eV. Notably,

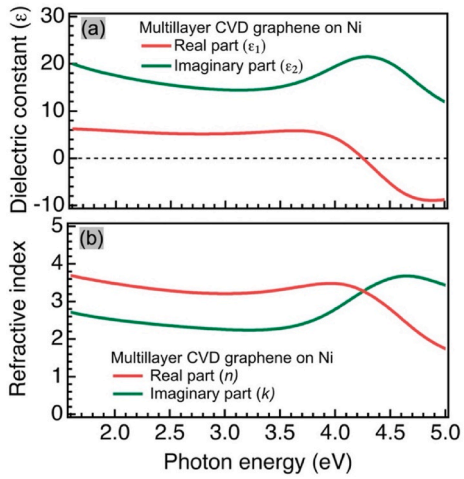

Fig. 4. (a) Complex dielectric constant and (b) Complex refractive index of multilayer CVD graphene on Ni.

ε_2 exhibited optical transitions with a distinctive narrow peak at 4.38 eV. The energy involved corresponds to the critical point linked to the van Hove singularity in the joint density of states, which is related to the interband transitions among $\pi \rightarrow \pi^*$ orbitals around the M point of the graphene Brillouin zone [2,7,41,72]. Trevisanutto et al. reported the occurrence of the $\pi \rightarrow \pi^*$ transition around 5 eV [53]. However, Yang et al. proposed the $\pi \rightarrow \pi^*$ transition occurring at 4.5 eV using GW + BSE, a method that considers both e-e and e-h interaction [52]. In Fig. 4(b), the obtained trends for refractive indices (n) and extinction coefficients (k) of multilayer graphene on Ni are illustrated, focusing mainly on the van Hove singularity region (4–5 eV). Beyond 1.6 eV, as photon energy rises, the extinction coefficient (k) initially decreases, followed by an increase, reaching its peak at approximately 4.8 eV. Concurrently, the refractive index (n) experiences a decline around this energy level.

The optical conductivity (σ_1) is linked to the imaginary part of the dielectric constant (ε_2). Fig. 5 illustrates the optical conductivity (σ_1) of multilayer graphene on Ni, showing a symmetrical peak at 4.38 eV. With the prediction calculation using the local density approximation method that only considers band-to-band transitions, the optical transition peak at 4.1 eV is obtained. Nevertheless, the projected optical transition peak shifts to 5.2 eV by integrating electron-electron interactions via the GW approach. Additionally, introducing electron-hole interactions foresees a 600 meV redshift in the optical transition peak, moving it from 5.2 eV to 4.6 eV [52]. The peak position of σ_1 for multilayer graphene on Ni, it occurs at 4.38 eV. By using Fano parameters ($q = -1.29$, $\Gamma = 0.89$ eV, and $E_{res} = 4.68$ eV), we can explain the phenomenon of the redshift seen in the peak, which initially occurred at 5.3 eV. However, the proposed model cannot match the notably symmetric shape of our data, as illustrated in Fig. 5. As a result, this suggests the minimal impact of the excitonic contribution to this observed redshift [23].

Fig. 6 illustrates the simplified energy band and optical transition states to clarify the measured optical conductivity and possibilities

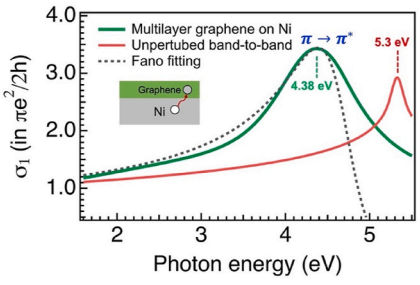

Fig. 5. The real part (σ_1) of optical conductivity (green lines) of multilayer CVD graphene on Ni with Fano line-shape analysis (black dashed lines). The $\sigma_{cont}(\omega)$ represents the unperturbed band-to-band transition, depicted by the red lines.

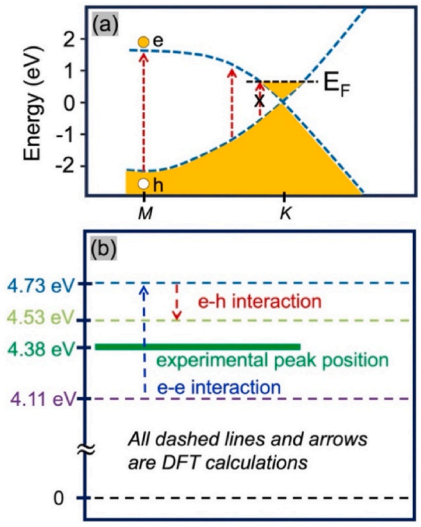

Fig. 6. (a) Illustration of the band diagram of graphene/Ni with considerable electron doping as predicted by DFT [72], and (b) Energy values for graphene/Ni that correspond to peak positions in the optical transitions.

transition in graphene/Ni based on projections obtained from DFT. These scenarios encompass two distinct processes: (i) significant charge transfer from the Ni to graphene, leading to electron doping [73], and (ii) the subsequent influence of this electron doping on the optical conductivity of graphene [72]. In theory, substantial shifts occur in the Fermi level upon deposition of graphene onto a metal substrate like Cu or Ni. These shifts are influenced by factors such as the interface between graphene/Ni and the work function of Ni [73]. Electron doping effectively shields e-h interactions while amplifying the impact of e-e interactions. As shown in Fig. 6(a), the red arrows indicate the potential transitions, which denote states that are higher than the Fermi level. Unreachable states are those above the Dirac point and below the Fermi level (shown by a crossed red arrow). When graphene interacts with a Ni substrate, it offers a shift in the Fermi level above the Dirac point. This result resembles the Fermi shift of 0.5 eV when graphene interacts with Cu substrates [73].

Fig. 6(b) presents an energy state diagram illustrating the peak positions within the optical transitions observed in graphene. The dashed lines and arrows in the graph correspond to electron-doped graphene based on theoretical predictions [72]. The purple dashed line at 4.11 eV corresponds to the results generated by the local density approximation principle, which explicitly considers band-to-band transitions. The light blue dashed line around 4.73 eV shows the prediction obtained from the GW model, which has a many-body e-e interaction. The light green dashed line at 4.53 eV represents the energy level based on the prediction with the GW + BSE approach by including the e-h interaction [72]. Our experimental findings demonstrate a 4.38 eV symmetric peak position in σ_1, demonstrated by the thick green line. However, due to the charge transfer and lattice mismatch between graphene and the Ni substrate in our case, the optical transition peak changes to 4.38 eV. The interaction between graphene/Ni substrate alters the number of available states below the Fermi level, leading to significant changes in electron density and the work function.

4. Conclusion

In conclusion, we have characterized the optical properties of multilayer graphene on nickel (Ni) substrates using spectroscopic ellipsometry. The general optical spectral behavior of the refractive index and dielectric function from infrared to visible energy ranges, along with the sharpness and intensity of the main peak, and the convergence toward the universal value of optical conductivity at infrared energies. We observe an optical transition through the optical conductivity peak around 4.38 eV. This peak is related to the interband transition from π to π^* orbitals at the M-point. This peak shifts from 4.6 eV (for free-standing graphene) to 4.38 eV, which is related to the charge transfer and work function of the Ni substrate and causes a change in the number of states below the Fermi level in graphene. An understanding of the optical properties of graphene on Ni is essential to fully utilizing its potential in various applications, particularly graphene-based optoelectronic devices.

CRediT authorship contribution statement

Hervin Maulina: Writing – original draft, Methodology, Investigation, Data curation. **Eri Widianto:** Writing – review & editing, Methodology, Formal analysis. **Emmistasega Subama:** Methodology, Formal analysis. **Muhammad Riswan:** Data curation. **Cipto Driyo:** Data curation. **Dwi Nugraheni Rositawati:** Data curation. **Fahrudin Nugroho:** Writing – review & editing, Validation, Supervision, Project administration. **Moh Edi Wibowo:** Writing – review & editing, Validation, Supervision, Software, Project administration. **Iman Santoso:** Writing – review & editing, Validation, Supervision, Project administration, Funding acquisition, Conceptualization.

Declaration of generative AI and AI-assisted technologies in the writing process

During the preparation of this work, the authors used ChatGPT to proofread the manuscript and improve the wording. After using this tool, the authors reviewed and edited the content as needed and take full responsibility for the content of the publication.

Declaration of competing interest

The authors declare that they have no known competing financial interests or personal relationships that could have appeared to influence the work reported in this paper.

Acknowledgements

This work receives financial support from "Riset dan Inovasi untuk Indonesia Maju (RIIM)", BRIN-Indonesia (Grant No. 12/II.7/HK/2023), “Kementerian Pendidikan, Kebudayaan, Riset, dan Teknologi” through the Fundamental Research scheme (Grant No. 2656/UN1/DITLIT/PT.01.03/2024), and the INSPIRASI Program (Grant No. 159/E/KPT/2023) provided by Indonesian Endowment Fund for Education Agency (LPDP). H. Maulina acknowledges “Kementerian Pendidikan, Kebudayaan, Riset, dan Teknologi” for supporting their graduate study through the BPI scholarship scheme.

Data availability

Data will be made available on request.

References

[1] A.K. Geim, K.S. Novoselov, The rise of graphene, Nat. Mater. 6 (2007) 183–191, https://doi.org/10.1038/nmat1849.
[2] A.H. Castro Neto, F. Guinea, N.M.R. Peres, K.S. Novoselov, A.K. Geim, The electronic properties of graphene, Rev. Mod. Phys. 81 (2009) 109–162, https://doi.org/10.1103/RevModPhys.81.109.
[3] K.F. Mak, M.Y. Sfeir, Y. Wu, C.H. Lui, J.A. Misewich, T.F. Heinz, Measurement of the optical conductivity of graphene, Phys. Rev. Lett. 101 (2008), https://doi.org/10.1103/PhysRevLett.101.196405.
[4] K.S. Novoselov, V.I. Fal'Ko, L. Colombo, P.R. Gellert, M.G. Schwab, K. Kim, A roadmap for graphene, Nature 490 (2012) 192–200, https://doi.org/10.1038/nature11458.
[5] C.R. Dean, A.F. Young, I. Meric, C. Lee, L. Wang, S. Sorgenfrei, K. Watanabe, T. Taniguchi, P. Kim, K.L. Shepard, J. Hone, Boron nitride substrates for high-

quality graphene electronics, Nat. Nanotechnol. 5 (2010) 722–726, https://doi.org/10.1038/nnano.2010.172.
[6] K.I. Bolotin, K.J. Sikes, Z. Jiang, M. Klima, G. Fudenberg, J. Hone, P. Kim, H. L. Stormer, Ultrahigh electron mobility in suspended graphene, Solid State Commun. 146 (2008) 351–355, https://doi.org/10.1016/j.ssc.2008.02.024.
[7] K.F. Mak, C.H. Lui, J. Shan, T.F. Heinz, Observation of an electric-field-induced band gap in bilayer graphene by infrared spectroscopy, Phys. Rev. Lett. 102 (2009), https://doi.org/10.1103/PhysRevLett.102.256405.
[8] K.J. Tielrooij, L. Piatkowski, M. Massicotte, A. Woessner, Q. Ma, Y. Lee, K. S. Myhro, C.N. Lau, P. Jarillo-Herrero, N.F. Van Hulst, F.H.L. Koppens, Generation of photovoltage in graphene on a femtosecond timescale through efficient carrier heating, Nat. Nanotechnol. 10 (2015) 437–443, https://doi.org/10.1038/nnano.2015.54.
[9] J. Zhou, Z. Ren, S. Li, Z. Liang, C. Surya, H. Shen, Semi-transparent Cl-doped perovskite solar cells with graphene electrodes for tandem application, Mater. Lett. 220 (2018) 82–85, https://doi.org/10.1016/j.matlet.2018.02.106.
[10] L. La Notte, E. Villari, A.L. Palma, A. Sacchetti, M. Michela Giangregorio, G. Bruno, A. Di Carlo, G.V. Bianco, A. Reale, Laser-patterned functionalized CVD-graphene as highly transparent conductive electrodes for polymer solar cells, Nanoscale 9 (2017) 62–69, https://doi.org/10.1039/C6NR06156G.
[11] V.D. Tran, S.V.N. Pammi, B.J. Park, Y. Han, C. Jeon, S.G. Yoon, Transfer-free graphene electrodes for super-flexible and semi-transparent perovskite solar cells fabricated under ambient air, Nano Energy 65 (2019), https://doi.org/10.1016/j.nanoen.2019.104018.
[12] I. Khrapach, F. Withers, T.H. Bointon, D.K. Polyushkin, W.L. Barnes, S. Russo, M. F. Craciun, Novel highly conductive and transparent graphene-based conductors, Adv. Mater. 24 (2012) 2844–2849, https://doi.org/10.1002/adma.201200489.
[13] H. Sung, N. Ahn, M.S. Jang, J.K. Lee, H. Yoon, N.G. Park, M. Choi, Transparent conductive oxide-free graphene-based perovskite solar cells with over 17% efficiency, Adv. Energy Mater. 6 (2016) 2–7, https://doi.org/10.1002/aenm.201501873.
[14] D.H. Shin, J.M. Kim, S.H. Shin, S.H. Choi, Highly-flexible graphene transparent conductive electrode/perovskite solar cells with graphene quantum dots-doped PCBM electron transport layer, Dyes Pigments 170 (2019) 107630, https://doi.org/10.1016/j.dyepig.2019.107630.
[15] S. Chen, L. Brown, M. Levendorf, W. Cai, S.Y. Ju, J. Edgeworth, X. Li, C. W. Magnuson, A. Velamakanni, R.D. Piner, J. Kang, J. Park, R.S. Ruoff, Oxidation resistance of graphene-coated Cu and Cu/Ni alloy, ACS Nano 5 (2011) 1321–1327, https://doi.org/10.1021/nn103028d.
[16] J.K. Holt, H.G. Park, Y. Wang, M. Stadermann, A.B. Artyukhin, C.P. Grigoropoulos, A. Noy, O. Bakajin, Fast mass transport through sub-2-nanometer carbon nanotubes, Science 312 (2006) 1034–1037, https://doi.org/10.1126/science.1126298, 1979.
[17] W.A. de Heer, C. Berger, X. Wu, P.N. First, E.H. Conrad, X. Li, T. Li, M. Sprinkle, J. Hass, M.L. Sadowski, M. Potemski, G. Martinez, Epitaxial graphene, Solid State Commun. 143 (2007) 92–100, https://doi.org/10.1016/j.ssc.2007.04.023.
[18] T.Y. Kim, C.H. Park, N. Marzari, The electronic thermal conductivity of graphene, Nano Lett. 16 (2016) 2439–2443, https://doi.org/10.1021/acs.nanolett.5b05288.
[19] R.R. Nair, P. Blake, A.N. Grigorenko, K.S. Novoselov, T.J. Booth, T. Stauber, N.M. R. Peres, A.K. Geim, Fine structure constant defines visual transparency of graphene, Science 320 (2008) 1308, https://doi.org/10.1126/science.1156965, 1979.
[20] K.F. Mak, C.H. Lui, T.F. Heinz, Measurement of the thermal conductance of the graphene/SiO2 interface, Appl. Phys. Lett. 97 (2010), https://doi.org/10.1063/1.3511537.
[21] G. Do Lee, C.Z. Wang, E. Yoon, N.M. Hwang, D.Y. Kim, K.M. Ho, Diffusion, coalescence, and reconstruction of vacancy defects in graphene layers, Phys. Rev. Lett. 95 (2005), https://doi.org/10.1103/PhysRevLett.95.205501.
[22] P. Neugebauer, M. Orlita, C. Faugeras, A.L. Barra, M. Potemski, How perfect can graphene be? Phys. Rev. Lett. 103 (2009) https://doi.org/10.1103/PhysRevLett.103.136403.
[23] P.K. Gogoi, I. Santoso, S. Saha, S. Wang, A.H. Castro Neto, K.P. Loh, T. Venkatesan, A. Rusydi, Optical conductivity study of screening of many-body effects in graphene interfaces, EPL (Europhysics Letters) 99 (2012) 67009, https://doi.org/10.1209/0295-5075/99/67009.
[24] E. Widianto, L.Z. Maulana, E. Suharyadi, A. Giglia, K. Koshmak, S. Nannarone, A. Rusydi, I. Santoso, High-energy excitonic effects in single-layer graphene, Phys. Rev. Mater. 8 (2024), https://doi.org/10.1103/PhysRevMaterials.8.065201.
[25] S.M. Kozlov, F. Viñes, A. Görling, Bonding mechanisms of graphene on metal surfaces, J. Phys. Chem. C 116 (2012) 7360–7366, https://doi.org/10.1021/jp210667f.
[26] A. Nagashima, N. Tejima, C. Oshima, Electronic states of the pristine and alkali-metal-intercalated monolayer graphite/Ni(111) systems, Phys. Rev. B 50 (1994) 17487–17495, https://doi.org/10.1103/PhysRevB.50.17487.
[27] A. Varykhalov, J. Sánchez-Barriga, A.M. Shikin, C. Biswas, E. Vescovo, A. Rybkin, D. Marchenko, O. Rader, Electronic and magnetic properties of quasifreestanding graphene on Ni, Phys. Rev. Lett. 101 (2008), https://doi.org/10.1103/PhysRevLett.101.157601.
[28] A. Grüneis, D.V. Vyalikh, Tunable hybridization between electronic states of graphene and a metal surface, Phys. Rev. B Condens. Matter 77 (2008), https://doi.org/10.1103/PhysRevB.77.193401.
[29] P. Sutter, M.S. Hybertsen, J.T. Sadowski, E. Sutter, Electronic structure of few-layer epitaxial graphene on Ru(0001), Nano Lett. 9 (2009) 2654–2660, https://doi.org/10.1021/nl901040v.
[30] W. Moritz, B. Wang, M.L. Bocquet, T. Brugger, T. Greber, J. Wintterlin, S. Günther, Structure determination of the coincidence phase of graphene on Ru(0001), Phys. Rev. Lett. 104 (2010), https://doi.org/10.1103/PhysRevLett.104.136102.
[31] J. Wintterlin, M.L. Bocquet, Graphene on metal surfaces, Surf. Sci. 603 (2009) 1841–1852, https://doi.org/10.1016/j.susc.2008.08.037.
[32] I. Pletikosić, M. Kralj, P. Pervan, R. Brako, J. Coraux, A.T. N'Diaye, C. Busse, T. Michely, Dirac cones and minigaps for graphene on Ir(111), Phys. Rev. Lett. 102 (2009), https://doi.org/10.1103/PhysRevLett.102.056808.
[33] A.L. Walter, S. Nie, A. Bostwick, K.S. Kim, L. Moreschini, Y.J. Chang, D. Innocenti, K. Horn, K.F. McCarty, E. Rotenberg, Electronic structure of graphene on single-crystal copper substrates, Phys. Rev. B Condens. Matter 84 (2011), https://doi.org/10.1103/PhysRevB.84.195443.
[34] M. Batzill, The surface science of graphene: metal interfaces, CVD synthesis, nanoribbons, chemical modifications, and defects, Surf. Sci. Rep. 67 (2012) 83–115, https://doi.org/10.1016/j.surfrep.2011.12.001.
[35] A. Dahal, M. Batzill, Graphene–nickel interfaces: a review, Nanoscale 6 (2014) 2548, https://doi.org/10.1039/c3nr05279f.
[36] L. Meng, Q. Sun, J. Wang, F. Ding, Molecular dynamics simulation of chemical vapor deposition graphene growth on Ni (111) surface, J. Phys. Chem. C 116 (2012) 6097–6102, https://doi.org/10.1021/jp212149c.
[37] F. Zheng, Y. Liu, C.L. Zhang, J. Wang, N. Dong, P. De Han, Y.X. Wu, Y.C. Wu, Direct chemical vapor deposition growth of graphene on Ni particles using solid carbon sources, Rare Met. 40 (2021) 2275–2280, https://doi.org/10.1007/s12598-020-01610-2.
[38] G. Paolicelli, M. Tripathi, V. Corradini, A. Candini, S. Valeri, Nanoscale frictional behavior of graphene on SiO2 and Ni(111) substrates, Nanotechnology 26 (2015), https://doi.org/10.1088/0957-4484/26/5/055703.
[39] X. Zang, Q. Zhou, J. Chang, K.S. Teh, M. Wei, A. Zettl, L. Lin, Synthesis of single-layer graphene on nickel using a droplet CVD process, Adv. Mater. Interfac. 4 (2017), https://doi.org/10.1002/admi.201600783.
[40] K.F. Mak, L. Ju, F. Wang, T.F. Heinz, Optical spectroscopy of graphene: from the far infrared to the ultraviolet, Solid State Commun. 152 (2012) 1341–1349, https://doi.org/10.1016/j.ssc.2012.04.064.
[41] K.F. Mak, J. Shan, T.F. Heinz, Seeing many-body effects in single- and few-layer graphene: observation of two-dimensional saddle-point excitons, Phys. Rev. Lett. 106 (2011), https://doi.org/10.1103/PhysRevLett.106.046401.
[42] J.W. Weber, V.E. Calado, M.C.M. Van De Sanden, Optical constants of graphene measured by spectroscopic ellipsometry, Appl. Phys. Lett. 97 (2010), https://doi.org/10.1063/1.3475393.
[43] A. Matković, U. Ralević, G. Isić, M.M. Jakovljević, B. Vasić, I. Milošević, D. Marković, R. Gajić, Spectroscopic ellipsometry and the Fano resonance modeling of graphene optical parameters, Phys. Scripta (2012), https://doi.org/10.1088/0031-8949/2012/T149/014069.
[44] A. Gray, M. Balooch, S. Allegret, S. De Gendt, W.E. Wang, Optical detection and characterization of graphene by broadband spectrophotometry, J. Appl. Phys. 104 (2008), https://doi.org/10.1063/1.2974096.
[45] G. Isić, Spectroscopic ellipsometry of few-layer graphene, J. Nanophotonics 5 (2011) 051809, https://doi.org/10.1117/1.3598162.
[46] V.G. Kravets, A.N. Grigorenko, R.R. Nair, P. Blake, S. Anissimova, K.S. Novoselov, A.K. Geim, Spectroscopic ellipsometry of graphene and an exciton-shifted van Hove peak in absorption, Phys. Rev. B Condens. Matter 81 (2010), https://doi.org/10.1103/PhysRevB.81.155413.
[47] F.J. Nelson, V.K. Kamineni, T. Zhang, E.S. Comfort, J.U. Lee, A.C. Diebold, Optical properties of large-area polycrystalline chemical vapor deposited graphene by spectroscopic ellipsometry, Appl. Phys. Lett. 97 (2010), https://doi.org/10.1063/1.3525940.
[48] W. Li, G. Cheng, Y. Liang, B. Tian, X. Liang, L. Peng, A.R. Hight Walker, D. J. Gundlach, N.V. Nguyen, Broadband optical properties of graphene by spectroscopic ellipsometry, Carbon N Y 99 (2016) 348–353, https://doi.org/10.1016/j.carbon.2015.12.007.
[49] K.K. Tikuišis, A. Dubroka, K. Uhlířová, F. Speck, T. Seyller, M. Losurdo, M. Orlita, M. Veis, Dielectric function of epitaxial quasi-freestanding monolayer graphene on Si-face 6H-SiC in a broad spectral range, Phys. Rev. Mater. 7 (2023), https://doi.org/10.1103/PhysRevMaterials.7.044201.
[50] H. Fujiwara, Spectroscopic Ellipsometry: Principles and Applications, John Wiley & Sons, Ltd, UK, 2007.
[51] H. Fujiwara, R.W. Collins, Spectroscopic ellipsometry for photovoltaics volume 1: fundamental principles and solar cell characterization. http://link.springer.com/10.1007/978-3-319-95138-6, 2018.
[52] L. Yang, J. Deslippe, C.H. Park, M.L. Cohen, S.G. Louie, Excitonic effects on the optical response of graphene and bilayer graphene, Phys. Rev. Lett. 103 (2009), https://doi.org/10.1103/PhysRevLett.103.186802.
[53] P.E. Trevisanutto, M. Holzmann, M. Côté, V. Olevano, Ab initio high-energy excitonic effects in graphite and graphene, Phys. Rev. B Condens. Matter 81 (2010), https://doi.org/10.1103/PhysRevB.81.121405.
[54] P.K. Gogoi, I. Santoso, S. Saha, S. Wang, A.H.C. Neto, K.P. Loh, T. Venkatesan, A. Rusydi, Optical conductivity study of screening of many-body effects in graphene interfaces. https://doi.org/10.1209/0295-5075/99/67009, 2012.
[55] Y.C. Chang, C.H. Liu, C.H. Liu, Z. Zhong, T.B. Norris, Extracting the complex optical conductivity of mono- and bilayer graphene by ellipsometry, Appl. Phys. Lett. 104 (2014), https://doi.org/10.1063/1.4887364.
[56] K.K. Tikuišis, A. Dubroka, K. Uhlířová, F. Speck, T. Seyller, M. Losurdo, M. Orlita, M. Veis, Dielectric function of epitaxial quasi-freestanding monolayer graphene on Si-face 6H-SiC in a broad spectral range, Phys. Rev. Mater. 7 (2023), https://doi.org/10.1103/PhysRevMaterials.7.044201.

[57] A.N. Toksumakov, G.A. Ermolaev, M.K. Tatmyshevskiy, Y.A. Klishin, A.S. Slavich, I.V. Begichev, D. Stosic, D.I. Yakubovsky, D.G. Kvashnin, A.A. Vyshnevyy, A. V. Arsenin, V.S. Volkov, D.A. Ghazaryan, Anomalous optical response of graphene on hexagonal boron nitride substrates, Commun. Phys. 6 (2023), https://doi.org/10.1038/s42005-023-01129-9.

[58] W. Li, G. Cheng, Y. Liang, B. Tian, X. Liang, L. Peng, A.R. Hight Walker, D. J. Gundlach, N.V. Nguyen, Broadband optical properties of graphene by spectroscopic ellipsometry, Carbon N Y 99 (2016) 348–353, https://doi.org/10.1016/j.carbon.2015.12.007.

[59] M.A. El-Sayed, G.A. Ermolaev, K.V. Voronin, R.I. Romanov, G.I. Tselikov, D. I. Yakubovsky, N.V. Doroshina, A.B. Nemtsov, V.R. Solovey, A.A. Voronov, S. M. Novikov, A.A. Vyshnevyy, A.M. Markeev, A.V. Arsenin, V.S. Volkov, Optical constants of chemical vapor deposited graphene for photonic applications, Nanomaterials 11 (2021), https://doi.org/10.3390/nano11051230.

[60] Y.C. Chang, C.H. Liu, C.H. Liu, Z. Zhong, T.B. Norris, Extracting the complex optical conductivity of mono- and bilayer graphene by ellipsometry, Appl. Phys. Lett. 104 (2014), https://doi.org/10.1063/1.4887364.

[61] I. Santoso, S.L. Wong, X. Yin, P.K. Gogoi, T.C. Asmara, H. Huang, W. Chen, A.T. S. Wee, A. Rusydi, Optical and electronic structure of quasi-freestanding multilayer graphene on the carbon face of SiC, EPL 108 (2014), https://doi.org/10.1209/0295-5075/108/37009.

[62] I. Santoso, R.S. Singh, P.K. Gogoi, T.C. Asmara, D. Wei, W. Chen, A.T.S. Wee, V. M. Pereira, A. Rusydi, Tunable optical absorption and interactions in graphene via oxygen plasma, Phys. Rev. B Condens. Matter 89 (2014), https://doi.org/10.1103/PhysRevB.89.075134.

[63] I.K. Agus Putra Dana, P.D. Jatmiko, E. Suharyadi, I. Santoso, A compact, modular, multi-wavelength (200-850nm) rotating-analyzer ellipsometer for optical constant characterization of nanostructured materials, Eur. J. Phys. 41 (2020) 65303, https://doi.org/10.1088/1361-6404/ab9b3e.

[64] R.M. Kaloari, E. Widianto, I.K.A.P. Dana, A. Lukmantoro, E. Suharyadi, T. Kato, S. Iwata, M.U. Absor, I. Santoso, Anomalous optical properties of bismuth ultrathin film using spectroscopic ellipsometry in the visible - ultraviolet range, Thin Solid Films 773 (2023) 139825, https://doi.org/10.1016/j.tsf.2023.139825.

[65] E. Widianto, Shobih, N.M. Nursam, M.Y. Hanna, K. Triyana, A. Rusydi, I. Santoso, Electronic correlations enhance optical absorption in graphene oxide-modified methylammonium lead iodide perovskite, J. Alloys Compd. 947 (2023), https://doi.org/10.1016/j.jallcom.2023.169634.

[66] M. Riswan, E. Widianto, N.I. Istiqomah, C. Driyo, M. Arifin, I. Santoso, E. Suharyadi, Tuning optical properties of Au thin film using electric field for surface plasmon resonance biosensor application, Opt. Mater. 150 (2024), https://doi.org/10.1016/j.optmat.2024.115221.

[67] W. Yan, L. Mao, P. Zhao, A. Mertens, S. Dottermusch, H. Hu, Z. Jin, B.S. Richards, Determination of complex optical constants and photovoltaic device design of all-inorganic CsPbBr 3 perovskite thin films, Opt Express 28 (2020) 15706, https://doi.org/10.1364/oe.392246.

[68] T.C. Asmara, I. Santoso, A. Rusydi, Self-consistent iteration procedure in analyzing reflectivity and spectroscopic ellipsometry data of multilayered materials and their interfaces, Rev. Sci. Instrum. 85 (2014) 123116, https://doi.org/10.1063/1.4897487.

[69] T.C. Asmara, I. Santoso, A. Rusydi, Self-consistent iteration procedure in analyzing reflectivity and spectroscopic ellipsometry data of multilayered materials and their interfaces, Rev. Sci. Instrum. 85 (2014) 123116, https://doi.org/10.1063/1.4897487.

[70] A.C. Ferrari, J.C. Meyer, V. Scardaci, C. Casiraghi, M. Lazzeri, F. Mauri, S. Piscanec, D. Jiang, K.S. Novoselov, S. Roth, A.K. Geim, Raman spectrum of graphene and graphene layers, Phys. Rev. Lett. 97 (2006), https://doi.org/10.1103/PhysRevLett.97.187401.

[71] A.C. Ferrari, D.M. Basko, Raman spectroscopy as a versatile tool for studying the properties of graphene, Nat. Nanotechnol. 8 (2013) 235–246, https://doi.org/10.1038/nnano.2013.46.

[72] L. Yang, Excitonic effects on optical absorption spectra of doped graphene, Nano Lett. 11 (2011) 3844–3847, https://doi.org/10.1021/nl201928g.

[73] G. Giovannetti, P.A. Khomyakov, G. Brocks, V.M. Karpan, J. Van Den Brink, P. J. Kelly, Doping graphene with metal contacts, Phys. Rev. Lett. 101 (2008), https://doi.org/10.1103/PhysRevLett.101.026803.